Miniature Permanent Magnet for Table-top NMR

GIORGIO MORESI,[1] RICHARD MAGIN[2]

[1] *Department of Physics and Astronomy, Institute of Physics, Condensed Matter Division, University of Basel, Klingelbergstrasse 82, CH-4056, Basel, Switzerland*
[2] *Department of Bioengineering, University of Illinois at Chicago, Science and Engineering Office Building (M/C 063), 851 South Morgan, Chicago, Illinois 60607-7052*

ABSTRACT: The multi-infinity dipole magnet is a new design capable of generating a relatively high and homogeneous permanent magnetic field (0.1–3 Tesla and homogeneity 20 ppm for 3 mm) that is suitable for nuclear magnetic resonance (NMR) or electron spin resonance (ESR) studies of small volume chemical or biological samples. The theoretical design and practical aspects involved in the construction of a prototype tabletop NMR system (0.6 T and homogeneity of 10 ppm in a ellipsoidal region of $3 \times 3 \times 5$ mm^3) are described. A simple NMR relaxation time experiment was performed on a water sample doped with 40 mM of $CuSO_4$. This system in its current configuration is suitable for relaxation time studies of materials or for educational use. The introduction of shim coils would increase the homogeneity of the magnet by a factor of 100, allowing the system to be used as a portable NMR spectrometer. In addition the introduction of gradient coils between the poles would transform the spectrometer to a MRI portable system for tissue analysis or simple MR microimaging at fields up to 3 T.
Concepts Magn Reson Part B (Magn Reson Engineering) 19B: 35–43, 2003

KEY WORDS: micro-imaging; microcoils; permanent magnet; Halbach; table-top spectrometer

INTRODUCTION

Magnetic resonance imaging (MRI) and nuclear magnetic resonance (NMR) spectroscopy are important diagnostic and analytical tools for biomedical studies. MRI provides submillimeter resolution of soft tissues in the body, whereas NMR spectroscopy is used for structural identification and kinetic studies of proteins, lipids, and carbohydrates. Both applications usually use large, cryogenically cooled superconducting magnets to establish the essential polarizing static B_0 field (typically 1.5 T for MRI and 11.7 T for NMR). Although low-field open MRI (0.6 T) and table-top relaxometers (0.25–1.5 T) use permanent magnets, such systems represent a small fraction of the total market. However, recent advances in permanent magnetic design (*1–6*) provide the basis for new table-top MRI and NMR systems for microimaging, relaxometry, microspectroscopy, and NMR process control. For example, the Halbach design, which generates a transverse field normal to the axis of an annular cylindrical magnet, is used by Hitachi in its R-1200 60-MHz spectrometer and by Progression, Inc. in NMR industrial process control systems (www.progression-systems.com). Large industrial versions of Halbach magnets (from 0.1 to 2 T for a 178 to 10-mm magnet bore, respectively) are available from Magnetic Solutions, Inc. (www.magnetic-solutions.com). In addition, a Halbach permanent magnet design was recently proposed by Maguire et al. (*7*) for use in a table-top NMR quantum computer.

Received 18 April 2003; revised 30 June 2003; accepted 1 July 2003

Correspondence to: Richard Magin, E-mail: rmagin@uic.edu

Concepts in Magnetic Resonance Part B (Magnetic Resonance Engineering), Vol. 19B(1) 35–43 (2003)

Published online in Wiley InterScience (www.interscience.wiley.com). DOI 10.1002/cmr.b.10082

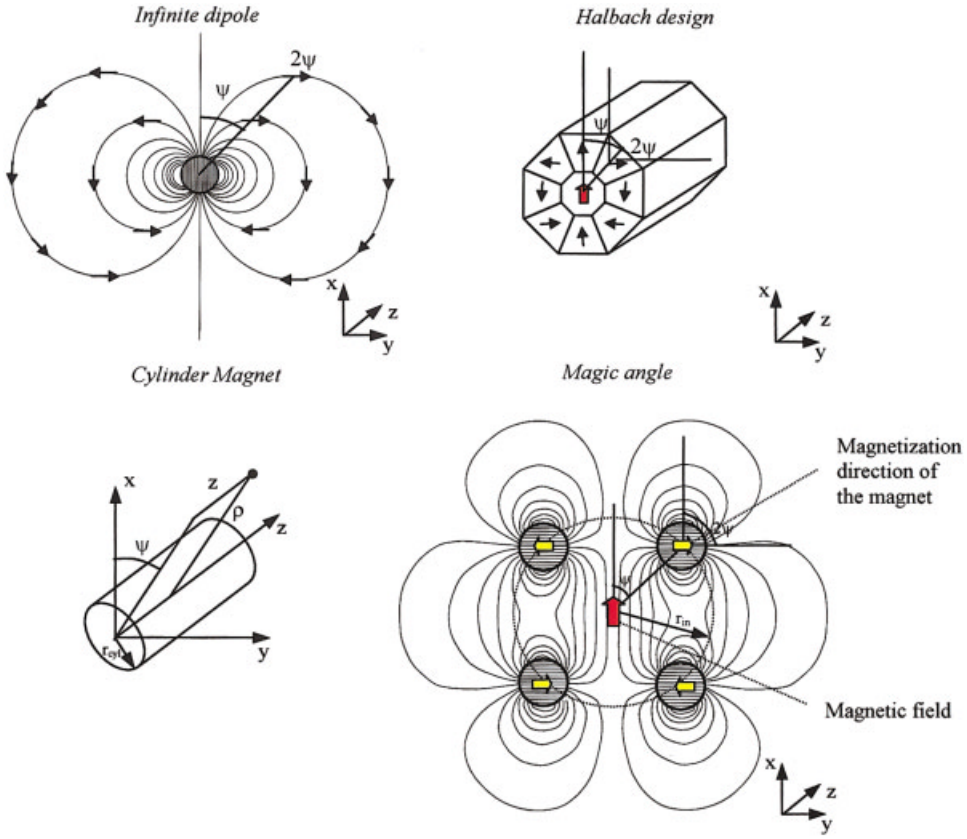

Figure 1 On the top left is represented the static magnetic field of the infinitesimal dipole and the resultant magnetic field generated in the *xy* plane; on the top right the Halbach design built from eight magnetic rectangular trapezoidal pieces. The magnetization of the segment follows the direction of a dipole placed in the center of the design. On the bottom left is represented the magnetic cylinder in cylindrical coordinates; in the bottom right is the theoretical static field in cross section at the middle of a four-cylinder Halbach design. [Color figure can be viewed in the online issue, which is available at www.interscience.wiley.com.]

In this article we describe a micro-NMR system based on the Halbach or "magic angle" design. A static field of 0.6 T with a homogeneity of 20 ppm was achieved in an elliptical volume of $3 \times 3 \times 5$ mm^3. The field could be increased to 3 T by adding a second layer of magnetic material, as some authors have demonstrated (*1, 2*).

BASIC PRINCIPLE

In most NMR spectrometer and MRI systems the static magnetic field, B_0, is directed along the central axis of the cylindrical magnet structure. Permanent magnets for open MRI typically employ parallel plate structures with B_0 directed normal to the parallel magnet poles. The Halbach permanent magnet design, however, is unique in that the orientation of the static field is traverse to the cylindrical axis, whereas the individual magnet segments are polarized in a direction out and around in a general dipole field arrangement as shown in Fig. 1. The key feature in its design is to place all the magnetic components around an infinity dipole with each segment of magnetic material oriented in the same direction as the field generated by a single dipole. In theory the direction of the magnetization for a segment with angular position ψ must 2ψ to model the ideal dipole field. Theoretical and numerical analysis by Halbach and Abele (*3, 5, 6*) demonstrate that the field generated inside the ideal structure is completely homogenous and the fringing is negligible.

For example, the B_0 static field in the air gap for a dipole cylinder of infinite length is given by Abele (*3*) as

$$B_y = J_r \ln\left(\frac{r_{out}}{r_{in}}\right) \qquad [1]$$

$$B_x \cong 0 \quad B_z \cong 0,$$

where r_{out} is the external radius, r_{in} is the internal radius and J_r the magnetic remanence of the material. Since in practice the cylindrical magnet structure is of finite length and must be assembled from different trapezoidal segments, two extra factors are introduced on the righthand of the equation: $\sin(2\pi/n)/(2\pi/n)$ to correct the segmentation of the magnetization around the dipole and $f(z)$ to correct the finite length of the cylinder.

In theory there is no limit to the magnitude of the static magnetic field that can be produced using the Halbach design, but in practice the coercitivity and anisotropy field of the magnet limit the ultimate performance to 3 T for the cylindrical configuration and 5 T for the spherical case (*3*). In addition the total magnetic field generated by the Halbach design can be oriented in the same direction (magnet positioned with an angle of $\psi = 0$) or in the opposite direction of the magnetization (magnet positioned with an angle $\psi = 90$) of the polarization of the individual components. In the second case, the strong magnetic field can consequently reverse the magnetization and demagnetize the magnet (*8, 9*). Although from a design perspective the trapezoidal magnet segments are almost ideal, in practice the difficulty and expense of machining and of orienting the polarization of each element limits the realization of this configuration. As an alternative, Skomski and Coey and others (*1, 3, 5, 6*) suggested the use of cylindrically shaped magnets that are magnetized transverse to their long axis. The field at the center of the magnet in this case is

$$B_0 = \frac{n}{2} J_r \frac{R^2}{r^2}, \qquad [2]$$

where n is the number of cylinders, R is the radius of each magnetic cylinder, r is the distance between the center of the "magic angle" design and the center of the cylinder segment, and J_r the magnetic remanence of the material. To correct the finite length, an $f(z)$ function also has to be introduced on the righthand side of the equation.

A key feature of the Halbach design is that such magnets can be nested without degrading the field of either source magnet, allowing the relative orientations of the fields from two Halbach designs to be smoothly varied by rotating one relative to the other. This feature also allows the total field from concentric Halbach magnets to be increased by superposition.

THEORY

One of the simplest ways of implementing a two-dimensional magnetic structure is to assume an infinitely long cylinder such as that show in Fig. 1. In this model two regions corresponding to radii $< r_{cyl}$ and radii $> r_{cyl}$ have to be considered. The medium inside the radius r_{cyl} is a homogenous magnetized material with a uniform remanence $\vec{J}_0$, and the medium outside the r_{cyl} is assumed to be free space with a permeability of μ_0. In a cylindrical system of coordinates ρ, ψ, z with the axis of the cylinder oriented in the direction of z $\vec{J}$, can be written in the form

$$\vec{J} = J_0(\cos(\psi)\vec{r} - \sin(\psi)\vec{\psi}). \qquad [3]$$

A z-independent solution of Laplace's equation for the scalar potential $\Phi(r, \psi)$ in cylindrical coordinates can be found by separation of variables (9) as

$$\Phi(r, \psi) = R(r)\cos\psi, \qquad [4]$$

where $R(r)$ satisfies the equation

$$r\frac{d}{dr}\left(r\frac{dR}{dr}\right) - R = 0, \qquad [5]$$

whose general solution is

$$R(r) = C_{i,1}r + C_{i,2}\frac{1}{r}. \qquad [6]$$

The sub indices i identify the regions:

$$i = 0 \quad \text{for } r < r_{cyl}$$

$$i = 1 \quad \text{for } r > r_{cyl}$$

and the four constants of integration $C_{i,1}$, $C_{i,2}$ are calculated using the boundary conditions at the interfaces between the regions of integration. First, because $\Phi(r, \psi)$ must be finite everywhere,

$$C_{0,2} = C_{1,1} = 0.$$

$$C_{0,1} = -\frac{J_0\ln(r_{cyl})}{2\mu_0} \qquad [7]$$

$$C_{1,2} = -\frac{J_0 r_{cyl}^2}{4\mu_0}. \qquad [8]$$

Consequently the magnetic flux density can be found by taking the negative gradient of the scalar potential:

$$\vec{B} = -\vec{\nabla}\Phi(r, \psi), \qquad [9]$$

for $r > r_{\text{cyl}}$

$$\vec{B} = \frac{J_0 r_{\text{cyl}}^2}{2r^2}\begin{pmatrix}\sin\psi \\ \cos\psi\end{pmatrix}\begin{pmatrix}\vec{r} \\ \vec{\psi}\end{pmatrix}. \qquad [10]$$

In this case we add N cylinders polarized by the Halbach rule, and find

$$\vec{B} = N\frac{J_0 r_{\text{cyl}}^2}{2r^2}\begin{pmatrix}\sin\psi \\ \cos\psi\end{pmatrix}\begin{pmatrix}\vec{r} \\ \vec{\psi}\end{pmatrix}. \qquad [11]$$

The correction of a finite system can be realized by introducing on the righthand of the equation a Bessel expansion function (*10*).

$$\vec{B} = N\frac{J_0 r_{\text{cyl}}^2}{2r^2}\begin{pmatrix}\sin\psi \\ \cos\psi\end{pmatrix}\begin{pmatrix}\vec{r} \\ \vec{\psi}\end{pmatrix}\cdot\frac{16}{\pi^2}\cdot\sum_{n,\vartheta}\frac{(-1)^{(\vartheta-1)/2}}{n\cdot\vartheta\cdot k_\vartheta(k_n r_{\text{cyl}})} \cdot\cos(\vartheta\cdot\psi)\cdot\sin(k_n\cdot z)\cdot k_\vartheta(k_n r) \qquad [12]$$

where the sum contains only n, ϑ odd integers and where k_ϑ is the Hankel function.

MAGNET DESIGN

A scale drawing and photograph of the prototype magnet is show in the Fig. 2. The magnet is constructed in an aluminum frame using eight cylindrical $SmCo_{17}$ magnets (Magnequench, Wayne, NJ). The individual cylindrical magnets are each 150 mm in length and 20 mm in diameter and are magnetized transverse to their long axis. Aluminum cylinder end pieces are glued with epoxy (Epotek ND 353) to both ends of the magnet element. The composite magnet element is then carefully inserted into a frame, and each magnet is rotated to the correct orientation using the aluminum end pieces and finally fixed with two screws pressing on the aluminum cylinder, as shown in Fig. 2. The main difficulty in this process is to introduce the magnet assembly into the frame without breaking or crushing the fragile ceramic-powder magnetic material. When all cylinders are inside the frame and properly aligned and fixed in place, the individual magnets are protected from damage and the structure is mechanically and thermally stable.

The magnet field in the active volume was scanned in x, y, z directions with a small (active area of 0.2×0.2 mm) Hall magnetic field probe (Magnetic Instruments Model 2010, Falmouth, Cornwall, UK). The static magnetic field was scanned while the cylinders were adjusted by rotating the transverse polarization to obtain the maximum static field homogeneity. When only four magnets are present in the frame, it is possible to access to the center of the magnet from the sides, but in the case of eight magnets, access is only possible from the ends.

Two iron plates are fixed on the aluminum frame using two screws, and in the gap a Teflon piece is introduced to allow access without contacting the frame of the assembly. The plates are introduced in the magnet and then fixed with another aluminum piece on the opposite end. The plates are turned to a position perpendicular to the magnetic field and fixed in place using screws. The function of the high-permeability ($\mu > 10{,}000$) plates is to improve the static field homogeneity by providing a uniform and homogenous material interface. A correction to the plates, suggested by Rose (*11–13*), was the introduction of small step ring (with a dimension of 0.2×0.1 mm) at each end to decrease the fringing field.

The plates were scanned in the x, y, z direction and adjusted using the four screws by optimizing the parallelism and separation distance. This operation was repeated until a field homogeneity of 20 ppm in a region of $3 \times 3 \times 5$ mm^3 was achieved. The peak magnetic field reached was 0.596 T. The dimensions of the inter plate volume are given by the gap between the plates: 5 mm height, 32 mm width, and 230 mm length.

The introduced plates produce an equipotential surface in the magnetic sense, and the variation of the field in x direction in the center of the structure is negligible. The highest variation of the magnetic field is in the y and z directions, and the graphs of the measured fields are plotted in Fig. 3 for the situation with and without the poles.

The experimental data, shown in Fig. 3, closely matches the static fields predicted by analytical calculation and numerical simulation corrected by adding an offset realized with the finite elements software (FEMM 3.2 and COSMOS).

In Fig. 3 the magnetic field homogeneity is plotted in the y and z axes (variation on the x axis not shown, because it is an order of magnitude smaller). The graphs show a variation of 20 ppm along the y axis for 3 mm and for the z axis one of 20 ppm for 5 mm. The homogeneity could not be calculated with such precision, in fact the realization shows a difference in homogeneity of a factor of 100. This large factor is

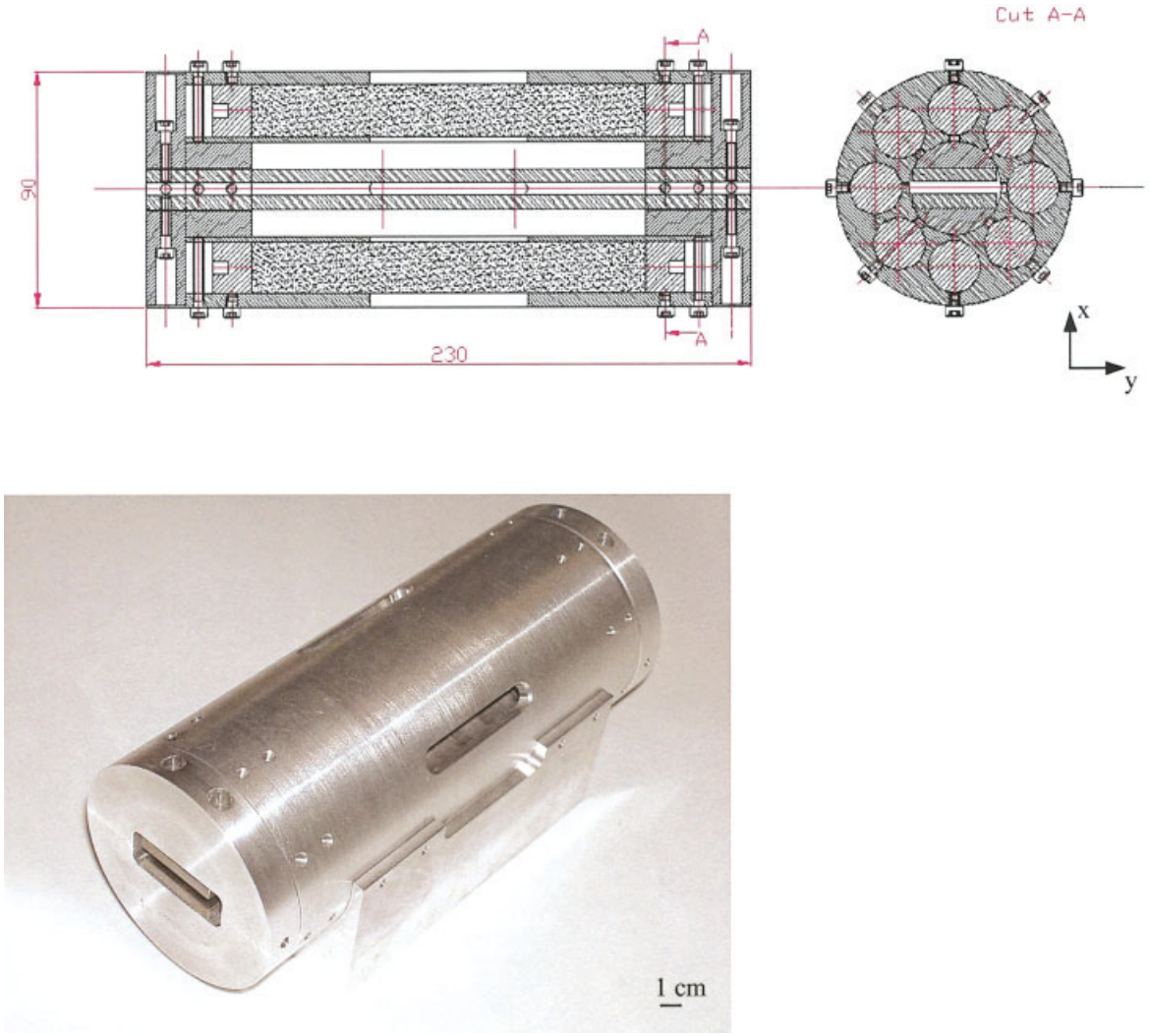

Figure 2 On the top is shown a scale drawing of the magnet designed with dimensions of 230 × 90 mm. The magnet is composed of eight $SmCo_{17}$ cylinders and two steel yokes in a frame of aluminum. On the bottom is the photograph of the physical magnet. [Color figure can be viewed in the online issue, which is available at www.interscience.wiley.com.]

caused by mechanical tolerances (±100 μm), placement (error in the orientation (±1°) and in the axial position (±500 μm) and quality of the material (magnetization and homogeneity).

EXPERIMENT

As an initial test of the prototype magnet, we conducted a simple NMR experiment using standard laboratory instruments configured as an NMR spectrometer. The solenoidal RF coil was wound around a 4-mm diameter glass capillary (8 turns of 650 μm diameter Kapton insulated copper wire, 5 mm of length). The coil had an inductance of 168 nH and an impedance of 0.29 Ω measured at the frequency of 25 MHz using an HP 8752A network analyzer. In parallel with the coil was connected an ATC ceramic capacitor (Model 181: 180 pF) and a Farnell trimmer capacitor (Model 499-432: 2–6 pF), which were soldered as close as possible to the coil for pretuning. In addition for matching, two capacitors, a ceramic (ATC, Model 470: 47 pF) and a trimmer (Farnell Model 499-432: 2–6 pF), adjusted for a value of 49 pF, were soldered to the coil assembly. The probe schematic and a photograph of the RF coil are shown in Fig. 4. A sample of pure water doped with 40 mM of $CuSO_4$ to decrease the T_1 and T_2 relaxation times to 45.5 ms (*14*) was introduced in a capillary.

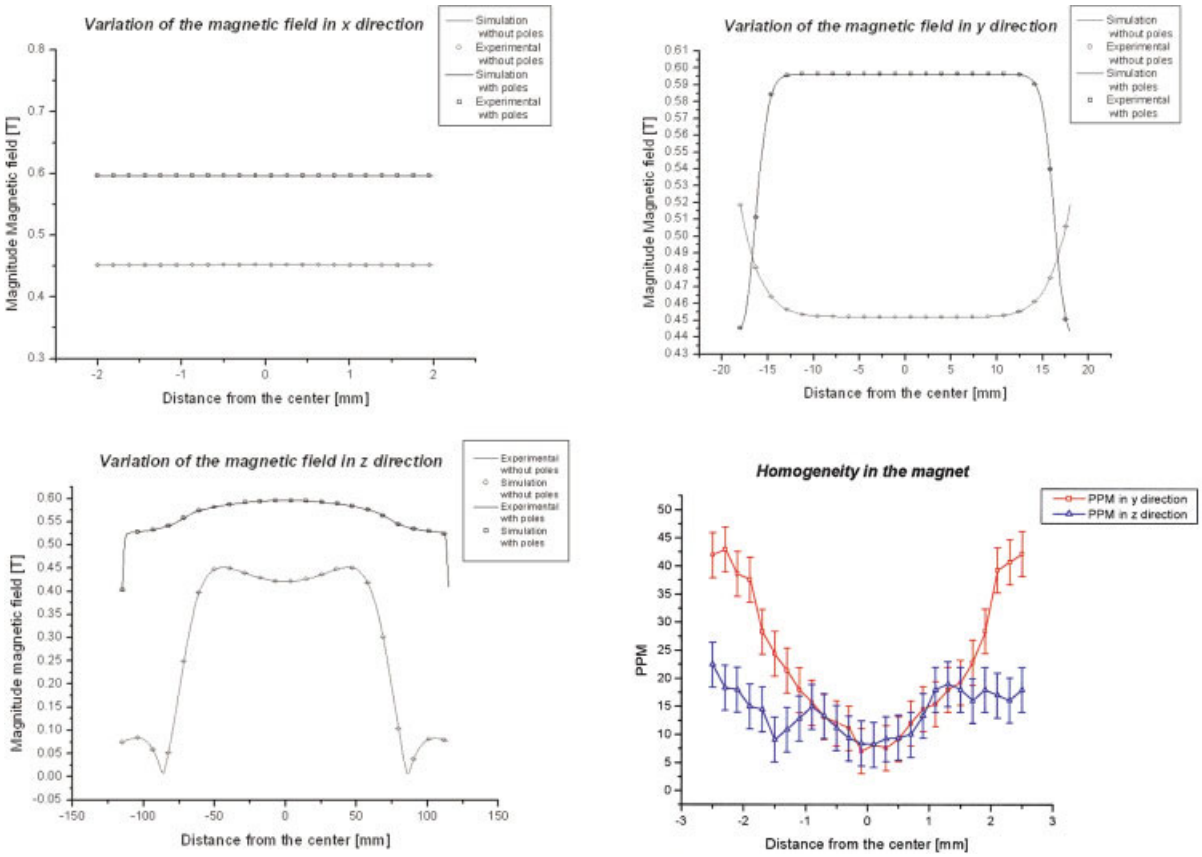

Figure 3 The graphs show the absolute value of the magnetic field in the x, y, and z directions. The solid lines represent the finite element simulation and the points the experimental results. The open circles correspond to the magnetic field measured without the poles present and the open boxes represent case when the poles are inserted. On the bottom right the figure shows the homogeneity of the magnetic field around the center of the magnet in ppm. [Color figure can be viewed in the online issue, which is available at www.interscience.wiley.com.]

The NMR probe was finally tuned and matched at the Larmor frequency of $f = 25.406$ MHz for a magnetic field of 0.5964 T, and a Q factor of 100 was measured. The coil was then positioned in the center of the magnet and no shimming or gradient coils were present.

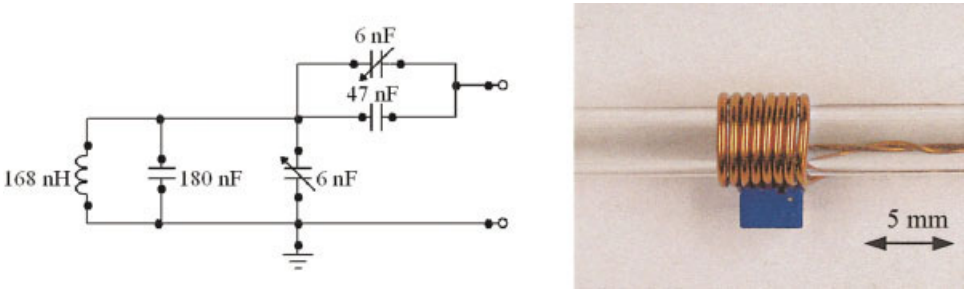

Figure 4 On the left is a schematic of the RF probe circuit consisting of the coil and 4 tune and match capacitors, and on the right is a photograph of the RF coil wound around a 4 mm diameter micro pipette glass capillary. The coil has 8 turns, an inner diameter of 4 mm and a length of 5 mm. The copper wire has a diameter of 600 μm and is insulated with Kapton. Below the coil a trim capacitor is soldered in parallel. [Color figure can be viewed in the online issue, which is available at www.interscience.wiley.com.]

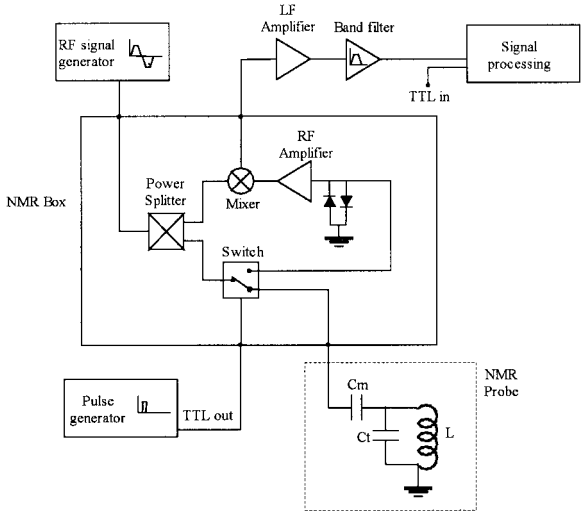

Figure 5 The schematic shows the excitation and detection system for the NMR system. The NMR probe, tuned and matched for the static magnetic field of 0.59 T is excited by a pulse sequence generated by the Standford DS345 pulse generator gating the RF pulse at the Larmor frequency. The signal is acquired, amplified by a factor of 100, mixed with the reference signal, amplified by another factor 100 and filtered with a bandwidth of 3–30 kHz before the digital signal processing.

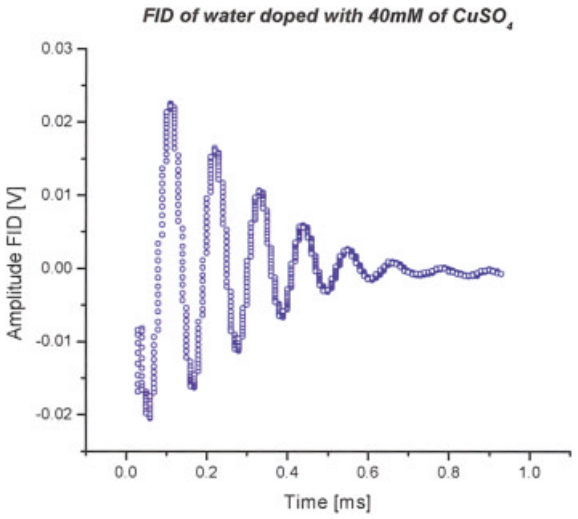

Figure 6 The graph shows the FID for 500 averages following a 90° pulse (20-μs duration for a power of 0 dBm) for an acquisition time of 20 ms and a repetition time of 150 ms. The observed decay in T_2^* corresponds to a Lorentzian linewidth of 1.06 kHz or at 0.6 T, a static field variation of 41.5 ppm. [Color figure can be viewed in the online issue, which is available at www.interscience.wiley.com.]

A schematic of the NMR excitation and detection system is shown in Fig. 5. The HP8648 signal generator was used to generate the RF signal at the Larmor frequency. The RF signal was pulse modulated by the Standford DS345 pulse generator. In order to isolate the RF amplifier from the excitation signal a TR switch (Minicircuits model ZASW-2-50DR) and a pair of a Schottky diodes (Siemens; model Bat-64) were used. The acquired RF signal (range μV) was amplified by 40 dB (Minicircuit amplifier model TIA-1000-IR8), demodulated with the mixer (Minicircuit ZAD-3), filtered with a bandwidth of 3–30 kHz and amplified at low frequency with a gain of 100 (Standford SR 560) before the digital signal processing was performed using a Labview A/D conversion card (PCI-mio-16e-1).

This simple NMR spectrometer design was adequate for this preliminary study after the ground loops were removed and when the electronic components were physically separated to minimize coupling. The noise measured using this NMR system was 2–3 times higher than the theoretical thermal noise generated by the coil. Thus, although not optimized, this design is an inexpensive compromise between price and performance, suitable for an instructional or portable NMR system.

An acquisition time of 20 ms was used for signal detection with a repetition time of 150 ms. The transmit pulse width was 20 μs with a power of 0 dBm applied to the NMR block to establish a 90° pulse. The detected signal (500 averages) is plotted in Fig. 6. The free induction decay occurs according to the system T_2^*, not the solution spin-spin relaxation time of 45.5 ms. Our results show a spin-spin relaxation time of 300 μs, corresponding to a factor of 150 increase in line broadening. This effect is caused by the nonhomogeneity of the static magnetic field. In fact assuming

$$\left(\frac{1}{T_2}\right)^* = \frac{1}{T_2} + \gamma \cdot \Delta B,$$

the magnetic field inhomogeneity, ΔB can be calculated as 41.5 ppm (*14*). These results show the importance of a shim system to decrease the line broadening and to provide better resolution and consequently, a higher signal-to-noise ratio.

In terms of magnet stability the system shows a shift in frequency of −300 ppm/K. This shift would be a major problem for coherent studies and for high-resolution spectroscopy. However, the frequency shift can be easily controlled by a frequency lock system or by immersion of the magnet in a stabilized temperature environment such as an oven.

DISCUSSION

The goal of this study was to design, build and test a prototype table-top permanent magnet NMR system. The prototype was realized as a first step toward building a portable NMR system operating at a magnetic field of 3 T. The system is designed to operate without any cryogens. Because of the high magnetic field inhomogeneity, there is only a small region within the magnet structure where NMR studies can be performed. In this study we used a solenoidal NMR microcoil (active volume approximately 50 μl) positioned at the center of the magnet. Such microcoils have been used in previous studies to acquire signals in an unshimmed cryogenic superconducting NMR magnet system (*15*). Microcoil technology offers significant advantages by reducing the volume over which the polarizing magnetic field must meet a specified homogeneity. This approach is advantageous for smaller, less-expensive NMR systems and has been proposed by others (*16, 17*). Moreover, the ability to fabricate planar microcoils on a chip, integrated with physical, chemical, and other analytic separation techniques, such as capillary electrophoresis, offers the potential for the development of inexpensive "moderate" resolution table-top NMR spectrometers.

The RF field sensitivity (B_1/I) of the detected NMR signal increases as the dimensions of the microcoil are reduced by the factor $1/\sqrt{d}$ (for d coil diameter $<$ 300 μm) and the homogeneity of the static magnetic field improves (*18–22*). However, the overall signal-to-noise will decrease with the sample volume because fewer spins are available. The absolute signal can be increased, or example, by using electrophoresis to concentrate a charged substance by a factor of 20–100 or more (*23–25*). Experimental NMR results demonstrated that without any shimming, the field was sufficiently homogenous to allow detection of a proton signal from a water sample doped with 40 mM of copper sulfate ($CuSO_4$) with a signal-to-noise ratio of 100 in 1 scan. Other approaches to table-top NMR systems (Bruker Minispect and NMR Mouse) are available (*26, 27*) for the investigation of chemicals, materials like elastomers, and biological tissue. In addition, Wright's group at Texas A&M University (*28*), has built a low-field NMR microimaging system for educational and industrial applications that has an in plane resolution of 150 × 150 μm. These systems, although promising, do not have the potential to reach the high and relatively homogenous fields that are theoretically possible with the Halbach design examined in this article.

CONCLUSIONS

The design, fabrication and testing of a compact prototype magnet for simple NMR relaxation and spectroscopy studies was demonstrated. A signal from a 62-μl sample of water doped with $CuSO_4$ was detected (SNR of 100 for a single scan) in a magnetic field of 0.6 T with a homogeneity $>$ 20 ppm. A key feature of this design is that the magnetic field can be increased up to 3 T by adding additional concentric layers of magnetic material. This result is promising and encourages us to develop shim and gradient systems to improve the field homogeneity for the development of second generation, table-top NMR spectrometers, and MR microimaging systems. Such instruments would be capable of serving a variety of needs in educational, industrial, and scientific applications.

ACKNOWLEDGMENTS

The authors gratefully acknowledge the assistance of Prof. Gary Friedman, Department of Electrical and Computer Engineering, Drexel University, for helpful discussions on the theoretical calculations and for assistance with the magnet design.

REFERENCES

1. Skomski R, Coey JMD. 1999. Permanent magnetism. Bristol and Philadelphia: Institute of Physics Publishing.
2. Bloch F, Cugat O, Toussaint JC, Meunier G. 1999. Approaches novatrices à la génération de champs magnétiques intenses: sources de flux à aimants permanents. J de Physique III European J Appl Phys 5:85.
3. Abele MG. 1993. Structures of permanent magnets. New York: John Wiley & Sons.
4. Leupold HA. 1996. Rare-earth iron permanent magnets. New York: Oxford University Press p 381–429.
5. Halbach K. 1981. Physical and optical properties of rare earth cobalt magnets. Nuclear Instrum Methods 187: 109–117.
6. Halbach K. 1980. Design of permanent multipole magnets with oriented rare earth cobalt material. Nuclear Instrum Methods 169:1–10.
7. Maguire Y, Boyden E, Gershenfeld N. 2000. Toward a table-top quantum computer. IBM Systems J 39:823–839.
8. Parker RJ. 1990. Advances in permanent magnetism. New York: Wiley and Sons.
9. Ewing JA. 1900. Magnetic Induction in Iron and other

Metals. London: The Electrician, Printing and Publishing Co.
10. Jackson JD. 1999. Classical Electrodynamics. New York: John Wiley & Sons.
11. Rose ME. 1938. Magnetic field corrections in the cyclotron. Phys Rev 53:715–719.
12. Ishikawa Y, Chikazumi S. 1962. Design of high power electromagnets. Tokyo: Institute for Solid State Physics.
13. Osborn JA. 1945. Demagnetizing factors of the general ellipsoid. Washington: Naval Ordnance Laboratory.
14. Viola L, Fortunato EM, Lloyd S, Tseng C-H, Cory DG. 2000. Stochastic resonance and nonlinear response using NMR spectroscopy. Phys Rev Lett 84:5466–5469.
15. Abragam A. 1961. The Principles of nuclear magnetism. London: Oxford University Press.
16. Wright AC, Neideen TA, Magin RL, Norcross JA. 1998. Evaluation of radio frequency microcoils as nuclear magnetic resonance detectors in low-homogeneity high-field superconducting magnets. Rev Sci Instrum 69:3938–3941.
17. Magin RL, Webb AG, Peck TL. 1999. Miniature magnetic resonance machines. IEEE Spectrum 34:51–66.
18. Webb A. 1997. Radio frequency microcoils in magnetic resonance. Progr Nuclear Reson Spectr 31:1–47.
19. Trumbull JD, Glasgow IK, Beebe DJ, Magin RL. 2000. Integrating microfabricated fluidic systems and NMR spectroscopy. IEEE Trans Biomed Engr 47(1).
20. Wu N, Peck TL, Webb AG, Magin RL, Sweedler JV. 1994. ^{1}H-NMR spectroscopy on the nanoliter scale for static and on-line measurements. Anal Chem 66:3849–3857.
21. Olson DL, Peck TL, Webb AG, Magin RL, Sweedler JV. 1995. High-resolution microcoil ^{1}H-NMR for mass-limited, nanoliter-volume samples. Science 270:1967–1970.
22. Peck TL, Magin RL, Lauterbur PC. 1995. Design and analysis of microcoils for NMR microscopy. J Magn Reson 108B:114–124.
23. Lichtenberg J, Verpoorte E, Rooij NF. 2001. Sample preconcentration by field amplification stacking for microchip-based capillary electrophoresis. Electrophoresis 22:258–271.
24. Peck TL, Magin RL, Lauterbur PC. 1995. Design and analysis of microcoils for NMR microscopy. J Magn Reson 108B:114–124.
25. Hoult DI, Richards RE. 1976. The signal to noise ratio of the nuclear magnetic resonance experiment. J Magn Reson 24:71–85.
26. Eidmann G, Savelsberg R, Blümler P, Blümich B. 1996. The NMR mouse: a mobile universal surface explorer. J Magn Reson 122:104–109.
27. Guthausen A, Zimmer G, Blümich B. 1997. Applications of the NMR mouse in material science. Proc. Conf. Low Resolution NMR, Sobottka J, editor. CD-ROM, DPG, Bad Honneff: 7 pp.
28. Wright SM, Brown DG, Porter JR, Spence DC, Esparza E, Cole DC, Huson FR. 2002. A desktop magnetic resonance imaging system. Magn Reson Materials Phys Biol Med 13:177–185.